Modeling of a Cottrell Atmosphere

David Gross

Jeliazko Jeliazkov

Bryce Thurston

Physics 466

5/7/13

Introduction

The concept of a Cottrell atmosphere is important to many aspects of materials science and engineering. This was first proposed by Cottrell and Bilby[1] in 1949 for the interaction of solute carbon atoms with defects in steels. These defects, one example being dislocations, produce long range elastic stress fields that distort the interstitial lattice sites around said defects. These distorted lattice sites then provide lower energy sites for the solute carbon to occupy, relieving some of the stress field. This raises the flow stress for the dislocation. More recently, the concept of a Cottrell atmosphere has been extended to the study of hydrogen embrittlement [2, 3]. Both the Hydrogen Enhanced Localized Plasticity (HELP) mechanism and the Hydrogen Induced Decohesion (HID) mechanism rely on localized excess of hydrogen accumulating in the elastic stress fields surrounding a defect. This defect is a dislocation for the HELP mechanism or a crack tip for the HID mechanism. These changes will lower the material's resistance to dislocation motion for the HELP mechanism, or crack advancement for the HID mechanism, causing subcritical failure of the material.

We have used atomistic modeling to explore the formation of a localized hydrogen atmosphere within the elastic stress field around a defect. This was achieved in two different steps. First, we used a Molecular Dynamics (MD) type simulation to create a defect and then allow the lattice to relax around the defect. We then compared the stresses on the sample to the theoretical stresses that would be around an edge dislocation to determine the accuracy of our model. The second step utilizes a Kinetic Monte Carlo (KMC) type simulation to allow hydrogen to diffuse through the sample. From this we examine how the distorted interstitial lattice sites allow for hydrogen interaction and look at the diffusion coefficients of hydrogen in our lattice.

Molecular Dynamics

For the MD simulation we chose to model an idealized two dimensional Fe lattice with either 21x21 atoms or 31x31 atoms. The 441 atom lattice was used for most analysis due to faster simulation time. The lattice was square in construction to simplify the modeling of the dislocation. A two dimensional lattice was utilized to speed up the procedure and because there is no out of plane strain from the dislocation[4], so the full three dimensional structure should be obtainable by extrapolation from this

lattice. Figure 1, a graph of the data points of the 21x21 lattice, shows the beginning lattice with no defects. The Fe-Fe interaction was accounted for by utilizing the Leonard-Jones type potential for Fe developed by Böyükata et al. [5seen here.

$$V\left(r_{ij}\right)=16.5\left[\left(\frac{2.517}{r_{ij}}\right)^{7}-\frac{7}{3.5}\left(\frac{2.517}{r_{ij}}\right)^{3.5}\right]$$

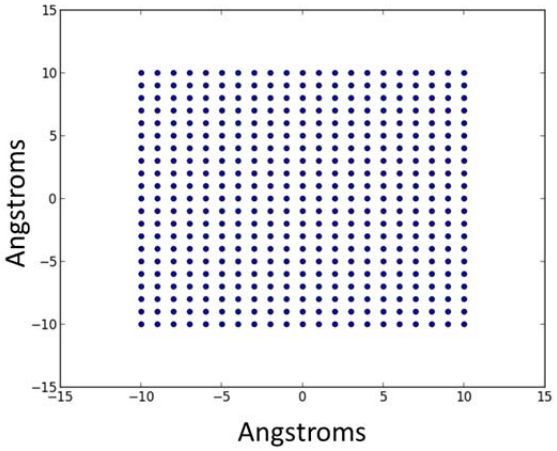

Figure 1: The 21x21 lattice with no defects

The potential is in terms kcal/mol and r_{ij} represents the interatomic separation distance. If this potential is used as is, the square lattice will not be stable. Instead, the sample will default into a hexagonal closed packed plane to minimize the free energy. To prevent this from happening and to stabilize the square lattice we will only consider nearest neighbor interactions as attractive. This meant that attractive forces were only transmitted within the planes of atoms presented on the two dimensional cross section. Other interactions will incorporate the repulsion term only if they approach closer than the equilibrium distance of 2.517 angstroms. This creates the appropriate reaction around the dislocation core that, according the concepts of the Peierls Nabarro theory [6], is necessary for dislocation motion. In this theory, the stress needed to produce dislocation motion is proportional to the stress needed to break the bond on the neighboring plane. The lower half of the plane then forms a new bond with the former half plane, while the upper portion now exists as the dislocation half plane.

Additionally, the bonding within the plane was considered directional within the plane, as opposed to the Leonard-Jones type potential which is a spherical force. The force vector was found by finding the vector between the two nearest neighbor atoms in the plane. The force vector is then applied in this planar direction, not the vector of separation between an atom and its neighbor. This simulates in-plane bonding, while allowing for localized plane bending. If the sample did not have two nearest neighbors, such as at the boundaries, the force vector was applied in the direction of the displacement between the atoms.

To facilitate accurate atomic positions and forces the boundary condition had to be chosen effectively to emulate the crystalline positions. Our simulation utilized fixed boundary conditions such that the corners and the dislocation half plane would not move in any direction. The outer boundaries were flexible in that they could move in plane of the boundary condition, but not outside of it. Initially, the box was run as a square of atoms, but the final boundary conditions utilized were slanted such that the lowest plane of atoms would be in equilibrium as would the top plane. This should produce the correct stress state, where the planes below the dislocation are in tension and the planes above the dislocation are in compression. Figure 3A, a plot of the atomic positions on the 21x21 lattice, and Figure 3B, another plot of the atomic position prior to the molecular dynamic simulations on the 21x21 lattice, shows the two differing sets of boundary conditions. The second boundary conditions were utilized for all the data presented here, though the KMC utilized the former boundary conditions.

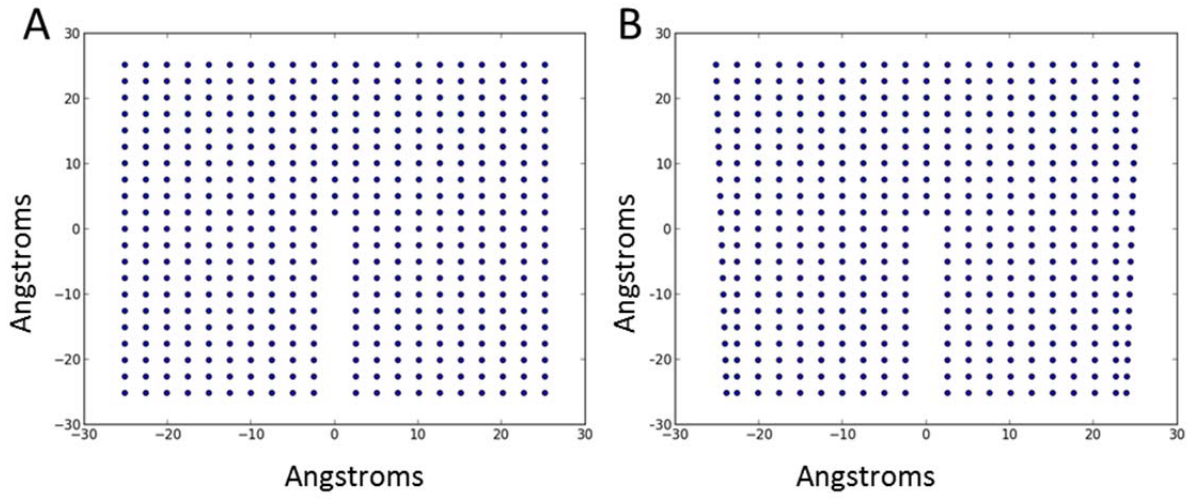

Figure 3: The depiction of two different sets of boundary conditions used, square (3A) and slanted (3B)

Since one of the goals of the simulation was to place the atoms into their lowest energy state the code utilized a progressive quench system to slowly remove the energy from the system. This manifested by allowing the code to run for 100 time steps with no limit on the energy of system to allow for all atoms to become slightly displaced. The system was then quenched by resetting all velocities to zero. The system was quenched again when the temperature of the system exceeded 600K. Subsequent quenches could occur in one of two ways. First, if the temperature exceeded half of the previous quench temperature, i.e. 300K for quench number 3, or 150K for quench number 4, the system was quenched. Second, if the system was not quenched for 1000 time steps it would be automatically quenched. Any subsequent temperature quench would then take this into account.

Figure 4 shows the total energy of the system as the 21x21 lattice relaxes. The material quickly relaxes into a lower energy state. The quenches can be seen on the as the discontinuities in Figure 4. The average total energy is approximately -26427.7 kcal/mol with a standard error of ±1.81 due to the nearest neighbor interactions. Figure 5A graphically demonstrates the final state of the following the relaxation and Figure 5B shows a superposition of the beginning and final state of the lattice.

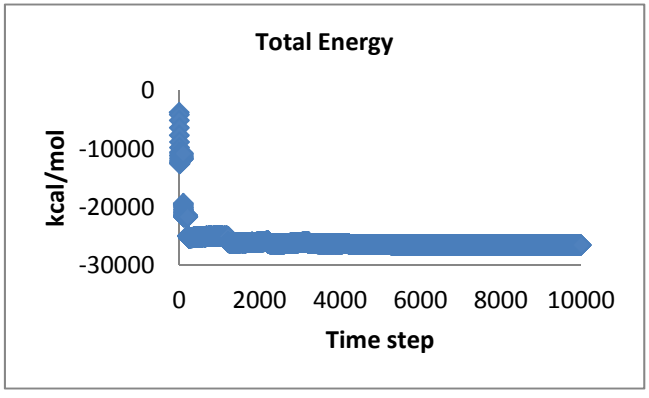

Figure 4: The total energy versus simulation time.

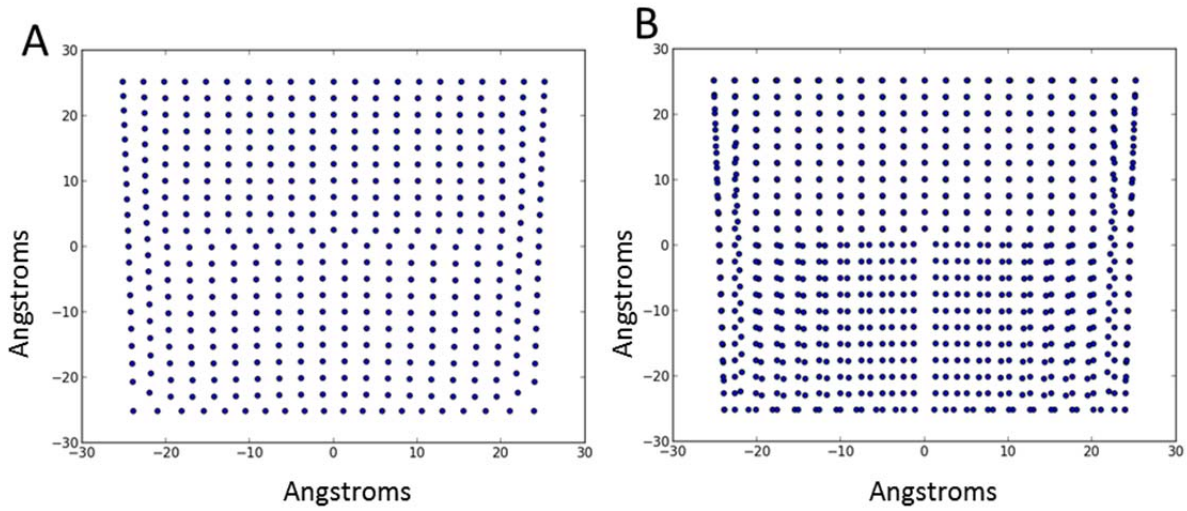

Figure 5: The final atomic positions (Figure 5A) and the superposition of the final atomic positions and the starting positions (Figure 5B)

During the test we summed the absolute value of the σ_{xx}, σ_{yy} and τ_{xy} forces on the particles and compared them to the theoretical stresses around the particle by using the equations presented by Foll [4]. To compute the experimental stress we assumed that the forces were acting on one half of a spherical particle. The average difference between the two forces was found. Table 1 shows the differences between the stresses. The difference between the average calculated forces and theoretical forces is small. There is a possibility that there was a strong influence due to the boundary conditions. Figure 6A shows the instantaneous σ_{yy} stress state following the simulation, while Figure 6B shows the theoretical stress state following the experiment. The boundaries of the simulation show a notably higher stress state than other portions. It may be possible to lower this with better boundary conditions, specifically fixing the positions such that the outer atoms are unable to move at all. It should also be noted that the theoretical stress states do diverge from the actual stress state close to the dislocation core.

Table 1: A comparison of the average stresses on an atom collected over 9000 data points (all in GPa)

	σ_{xx}	Error σ_{xx}	σ_{yy}	Error σ_{yy}	τ_{xy}	Error τ_{xy}
Simulated Average	2.27	±0.03	2.54	±0.05	3.94	±0.06
Theoretical Average	3.18	±0.13	1.09	±0.07	1.20	±0.12
Difference	-0.91	±0.13	1.45	±0.10	2.74	±0.15

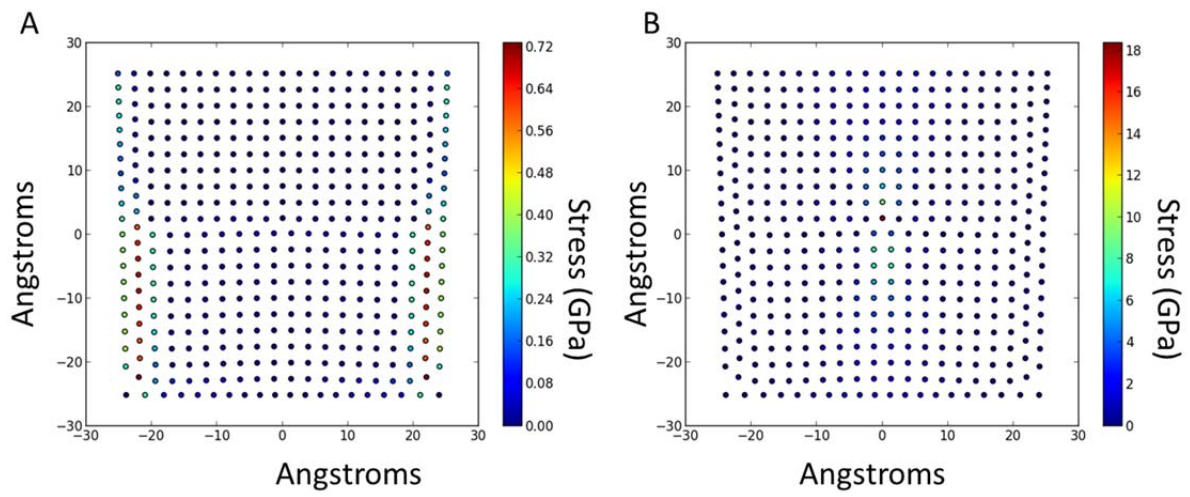

Figure 6: Stress of the experimental (6A) and the theoretical stress state. Figure 6A shows that boundary conditions play a large role. Figure 6B suggests that stress should be concentrated at the interface, but divergence is a known issue.

Additionally, the 31x31 lattice was simulated using the square boundary conditions, though it was not as robust a simulation since fewer steps were used in an effort to lower the computation time.

Kinetic Monte Carlo

Having determined the accuracy of the lattice resulting from the relaxation of an ideal defect, we then simulate the diffusion of hydrogen through this lattice.

First, we determine the potential necessary to use for this process. The literature on the subject indicates that the tetrahedral interstitial sites in a BCC lattice are the most energetically favorable for hydrogen [7]. These sites are shown in Figure 7.

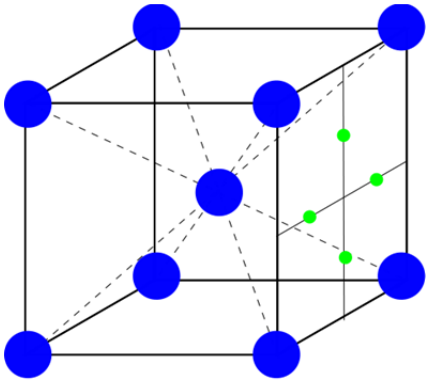

Figure 7: A BCC lattice with the tetrahedral interstitial sites marked in green.

Using the minimization finding techniques later explained, it was determined that an entirely repulsive potential makes these points the local minima in the potential energy landscape. As a result, the repulsive term in the Leonard-Jones potential is the term used to describe the interactions of the diffusing atoms with the lattice.

This potential is very short ranged so the contributions made to the potential energy at a specific point from far away atoms will be negligible. As a result the lattice was divided into cells. The potential energy at a point in a given cell was calculated using only the atoms in that and all neighboring cells (adjacent and diagonal).

The lattice of atoms creates a potential energy landscape with many local minima separated by potential energy barriers. As the particles diffuse through the lattice, they will spend much of their time vibrating in a specific potential energy minimum. It is only on longer timescales that the atoms will hop to neighboring minima. The thermal vibrations within a given stable position are not the focus of this study, so we required a method that would give us information on the transitions from one minimum to another. As a result, Kinetic Monte Carlo was chosen. It allows for the exploration of the occupancy over time as well as the option of calculating diffusion coefficients.

The next step in this method was to determine the stable points between which the atoms would diffuse. To do this the locations of the stable points needs to be determined. This had no simple geometric solution due to the use of a non-ideal lattice. Instead, we check points near each lattice atom and search for the nearest local minimum in potential energy. This search was conducted using the method of steepest descent. The step size taken during the search is scaled by the magnitude of the gradient and is limited by a maximum step size to prevent the program from overshooting the minimum. The list of grid points that is produced contains duplicates found from the fact that multiple points may have yielded the same local minimum. These duplicates were thus filtered from the list of grid points by eliminating any grid points located too close together. After doing this process, the KMC grid is obtained. A graphical depiction of it can be seen in Figure 8.

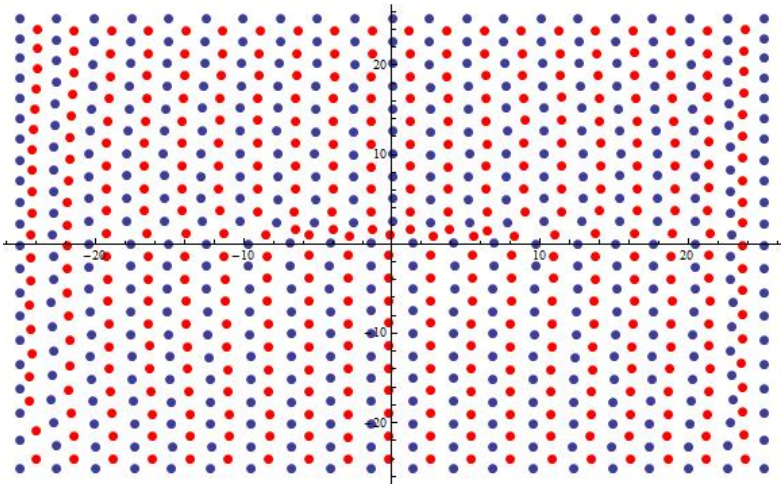

Figure 8: The blue points are the obtained atom locations and the red points are the determined locations for the KMC grid points.

From this list of KMC grid points, the neighbors of each then needed to be established. This was accomplished by first creating a list of possible neighbors for each grid point that met the criterion of being under a maximum distance away from a given grid point. However, some of the points obtained are unphysical due to the existence of an intermediate KMC grid point. To remove such points, the list of neighbors to each KMC point was filtered by putting a cap on the value of the dot product of the unit vectors in the directions to each possible nearest neighbor from a given point. When this cap was exceeded by two possible neighbors, the one the greatest distance away was removed from the list.

This establishes a list of neighboring points to which a particle can diffuse from one point. The rate at which it diffuses from point to point is the necessary piece of information in order to implement Kinetic Monte Carlo. Transition rate theory tells us that the rate at which the particle will transition from an equilibrium state to a saddle point is given by [8]:

$$\Gamma = \tilde{\nu} e^{-\frac{\Delta E}{k T}}$$

where ΔE is the energy difference between the energy at the peak of the potential barrier and the energy minima at the grid point. We then needed to calculate the peak potential energy between each grid point and its neighbors. This was done by scanning from each grid point to its neighbors and continually narrowing the scanning range around the maximum value of potential energy between the two.

We are then able to carry out the Kinetic Monte Carlo simulation. We use the n-fold way and so take a cumulative sum of all possible transition rates out of a given state:

$$R_i = \sum_{j=1}^{i} k_j$$

A random number u_1 is then generated on the interval (0, 1] and the selected rate is given by

$$R_{i-1} < u R_N \leq R_i$$

The transition rate that satisfies this equation corresponds to the transition made to evolve the system. Finally, the elapsed time is updated by

$$t = -\frac{\ln(u_2)}{R_N}$$

where u_2 is another random number on the interval (0,1].

This process is implemented by randomly selecting grid points corresponding to the number of hydrogen atoms in the simulation and placing atoms at these sites. A list is generated to store the location of each hydrogen atom as well as its corresponding transition rates. When a transition is made, this list and R_N are updated.

The amount of time the atoms spent in a given bin between steps is summed in a two dimensional histogram. Below are shown contour plots of lattices of two different sizes for the visualization of the histograms obtained from the previously described methods. It is clear from these that the most occupied sites are the ones that were more highly strained by the dislocation.

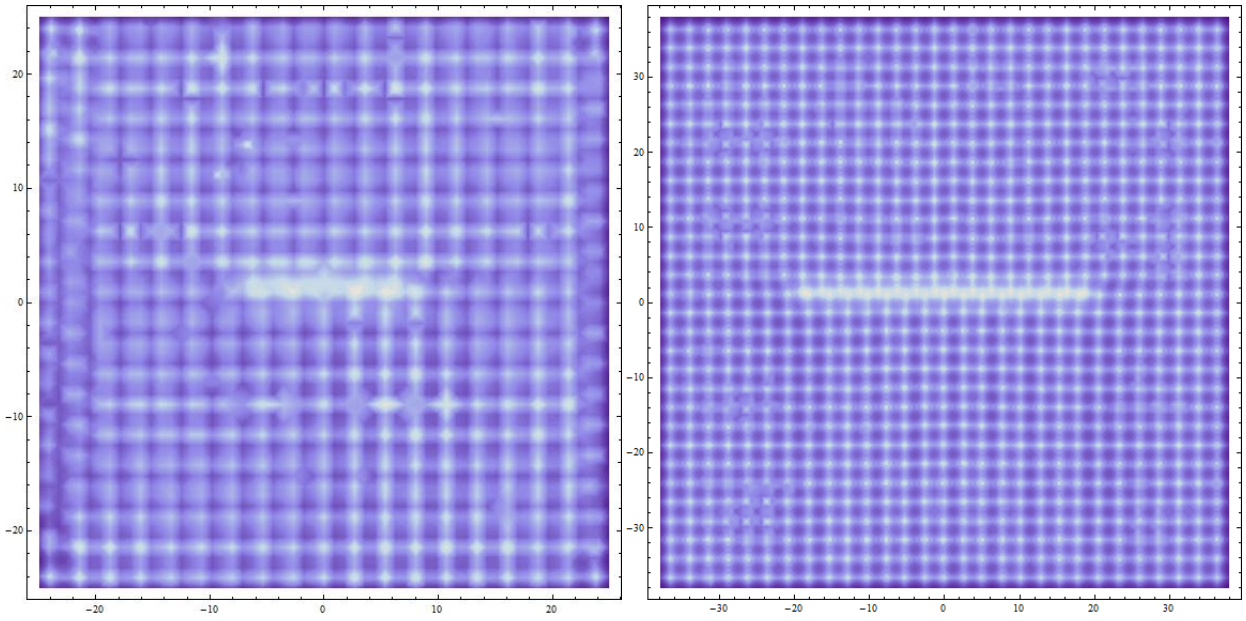

Figure 8: Above are shown graphical representations of the histograms of the occupancy time for initial atom grids of 21x21 and 31x31 respectively. Lighter colors mean higher occupancy. Units are in Å

Finally, we calculate diffusion coefficients for the system. This is done using Einstein's relation in two dimensions:

$$D = \lim_{t\to\infty} \frac{1}{4t} \langle |r(t) - r(0)|^2 \rangle$$

One issue with this formula in our circumstance is that it will vanish eventually as t goes to infinity since our system is finite. We then proceed by analyzing D as it depends on both the number of hydrogen atoms in our lattice and the time at which we calculated the diffusion coefficient.

We would expect the point at which the finite nature of the system is being overwhelmed by increasing time without bound to be the maximum in these plots. The results of this assumption are summarized in the following table. The errors reported are only the results of statistical error across the different particles.

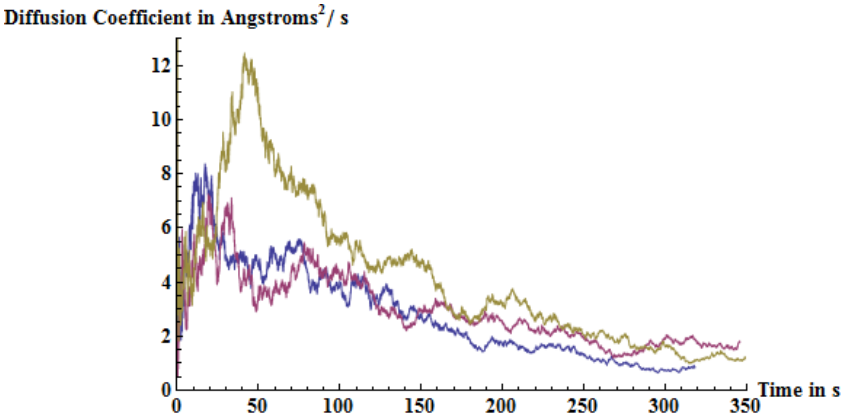

Figure 9: Plots of diffusion coefficients for our 31 by 31 lattice vs. time. This includes plots for 10 atoms (blue), 9 atoms (maroon), and 8 atoms (yellow).

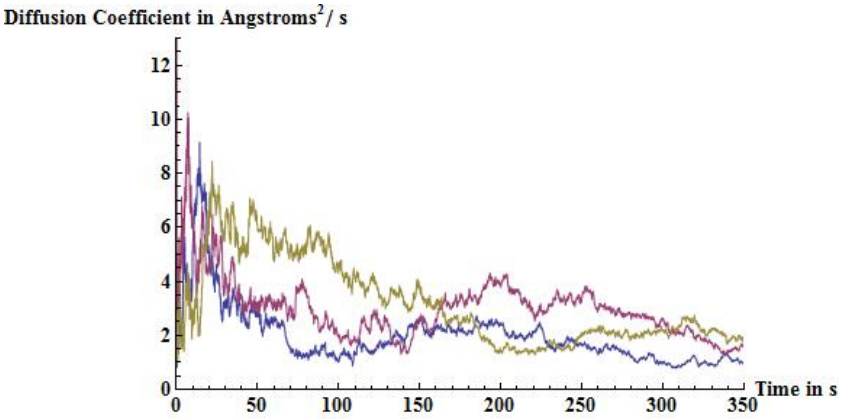

Figure 10: Plots of diffusion coefficients for our 31 by 31 lattice vs. time. This includes plots for 7 atoms (blue), 6 atoms (maroon), and 5 atoms (yellow).

Table 2: Diffusion coefficients for different numbers of atoms

Number of atoms	Calculated diffusion coefficient in $\text{Å}^2/\text{s}$
5	8.19 ± 0.220
6	10.08 ± 0.640
7	9.15 ± 0.555
8	12.46 ± 0.527
9	7.12 ± 0.446
10	8.23 ± 0.418

Conclusions/Future Work

We have presented a MD model utilizing a Leonard-Jones type potential for simulating the strained atomic planes around a planar defect. The forces involved are accurate to within an order of magnitude despite issues with boundary conditions and the theoretical equations divergence as the dislocation

core is approached. This lattice was then used for a KMC simulation of hydrogen diffusion demonstrating that preferred interstitial lattice sites are immediately around the dislocation core, in agreement with theories of hydrogen embrittlement, as well as calculated hydrogen diffusion constants for this lattices. Future work would involve utilizing more advanced potentials, including embedded atom potential and density functional theory for the MD and KMC simulation respectively for more accurate simulations. Additionally, the boundary conditions of the MD simulation could be refined and hydrogen-hydrogen interaction could be incorporated into the KMC simulation. The final goal, would be to extend the two dimensional treatment presented to three dimensions to more accurately model the atomic positions of hydrogen.

Works Cited:

1. Cottrell, A.H. and B.A. Bilby, *Dislocation Theory of Yielding and Strain Ageing of Iron.* Proceedings of the Physical Society. Section A, 1949. **62**(1): p. 49.
2. Birnbaum, H.K. and P. Sofronis, *Hydrogen-enhanced localized plasticity—a mechanism for hydrogen-related fracture.* Materials Science and Engineering: A, 1994. **176**(1–2): p. 191-202.
3. Lee, S.L. and D.J. Unger, *A decohesion model of hydrogen assisted cracking.* Engineering Fracture Mechanics, 1988. **31**(4): p. 647-660.
4. Foll, H., *Defects in Crystals*: http://www.tf.uni-kiel.de/matwis/amat/def_en/index.html.
5. Böyükata, M., et al., *Size evolution of structures and energetics of iron clusters: Molecular dynamics studies using a Lennard–Jones type potential.* Journal of Alloys and Compounds, 2005. **403**(1–2): p. 349-356.
6. Nabarro, F.R.N., *Dislocations in a simple cubic lattice.* Proceedings of the Physical Society, 1947. **59**(2): p. 256.
7. You, Y. et al, *Dissolving, trapping and detrapping mechanisms of hydrogen in bcc and fcc transition metals.* AIP Advances, 2013. **3**, 012118.
8. Vineyard, G.H. *Frequency Factors and Isotope Effects in Solid State Rate Processes*. J. Phys. Chem. Solids **3**, 121 (1957).